IEICE TRANS. INF. & SYST., VOL.E105–D, NO.5 MAY 2022

LETTER

Fully Connected Imaging Network for Near-Field Synthetic Aperture Interferometric Radiometer

Zhimin GUO[†a)], ***Member***, **Jianfei CHEN**[†], ***and*** **Sheng ZHANG**[†], ***Nonmembers***

SUMMARY Millimeter wave synthetic aperture interferometric radiometers (SAIR) are very powerful instruments, which can effectively realize high-precision imaging detection. However due to the existence of interference factor and complex near-field error, the imaging effect of near-field SAIR is usually not ideal. To achieve better imaging results, a new fully connected imaging network (FCIN) is proposed for near-field SAIR. In FCIN, the fully connected network is first used to reconstruct the image domain directly from the visibility function, and then the residual dense network is used for image denoising and enhancement. The simulation results show that the proposed FCIN method has high imaging accuracy and shorten imaging time.

key words: *fully connected, near field, synthetic aperture radiometer, imaging algorithm, sparse reconstruction*

1. Introduction

The millimeter wave synthetic aperture interferometric radiometers (SAIR) are very efficient instruments for obtaining high-precision images [1]. Benefit from synthetic aperture technology, SAIR utilize small aperture antenna array to compose large aperture synthetic antenna, so as to achieve high imaging precision,which is difficult to be realized by other systems [2]. Compared with infrared, millimeter waves have longer wavelengths and better penetrability. Compared with microwaves, millimeter waves have shorter wavelengths and higher imaging resolution. In the early days, SAIR was utilized primarily in the fields of radio astronomy and earth remote sensing [3]. With the changes in the global counter-terrorism situation in recent years, SAIR is gradually introduced into the near-field imaging due to the advantages and safety of technology of SAIR.

The traditional synthetic aperture imaging algorithm meets the premise of far-field interferometry [4], but in the near-field, the visibility function measured by SAIR and the brightness temperature distribution of the target scene no longer meet the Fourier transform relationship. The traditional imaging algorithm is difficult to achieve the ideal effect for the near-field SAIR. At present, there are two kinds of near-field algorithms. One is the Fourier transform method based on phase correction, such as modified FFT (MFFT) method [5]. By adding the correction phase, MFFT method makes the visibility function and the brightness temperature distribution meet the approximate Fourier transform to obtain the equivalent far-field imaging conditions. The second is the inversion method based on G-matrix, which models the complex synthetic aperture imaging process as a mathematical model and inverses the brightness temperature distribution of the target scene by solving the G-matrix method [6]. In these two methods, the reconstruction of the target image is optimized by numerical inversion method, based on the establishment of their inversion model. Owing to the inevitable factors such as noise interference and system parameters error, there are some errors in the model itself, so it is difficult to reconstruct an accurate millimeter wave image. In 2019, Zhang proposed the SAIR-CNN [7] algorithm based on learning super-resolution idea and realized better millimeter wave synthetic aperture imaging inversion results. Through deep learning, the imaging network obtained by SAIR-CNN is closer to the actual imaging and the model error is lower. Compared with traditional imaging inversion methods, SAIR-CNN method has a better effect on image quality and noise suppression. However, SAIR-CNN has not meant deeply studied for the particularity of near-field SAIR and realizes equal dimensional imaging inversion. In the practical near-field SAIR, due to the limitation of antenna array structure, the measured visibility function is usually sparse function, and disturbed by near-field spherical wave and serious multipath effect, its measurement error is usually large. Therefore, SAIR-CNN is difficult to realize image reconstruction for near-field SAIR.

Inspired by the SAIR-CNN algorithm, we proposed a novel FCIN to realize higher-precision imaging inversion for near-field SAIR with sparse visibility function. In the paper, we use feedforward neural network with higher optimal precision to complete the imaging inversion from sparse visibility function, then combine the residual dense network to complete the denoising and enhancement of millimeter-wave images. Finally, the experimental simulation results also show that in the case of near-field imaging, compared with the existing near-field imaging methods, the FCIN method has certain advantages in imaging accuracy and reconstruction time, which reflect that the FCIN is efficient and feasible.

Manuscript received November 17, 2021.
Manuscript revised January 24, 2022.
Manuscript publicized February 9, 2022.
[†]The authors are with Dept. of College of Electronic and Optical Engineering, Nanjing University of Posts and Telecommunications, Nanjing, China.
a) E-mail: 1220024222@njupt.edu.cn
DOI: 10.1587/transinf.2021EDL8105

2. Fully Connected Network Imaging Algorithm of Near-field SAIR

2.1 Synthetic Aperture Imaging Algorithm

Before discussing the near-field millimeter wave imaging method based on the fully connected network, the principle of millimeter wave synthetic aperture imaging is briefly reviewed. As shown in Fig. 1, the radiation source S is located on the plane oxy and is dispersed into N small parts. The antenna is located on the OXY. The distance between the point radiation source and the antenna is R_n^c and R_n^ι. According to [8], the visibility function of the antenna can be expressed as:

$$\begin{aligned} V_{c,\iota} &= <E_c(R_n^c, t) \bullet E_\iota^*(R_n^\iota, t)> \\ &= \sum_{n=0}^{N} T(n) F_c(x_n, y_n) F_\iota^*(x_n, y_n) e^{-jk(R_n^c - R_n^\iota)} \end{aligned} \tag{1}$$

Where $E_\#(t)$ is the scene radiation signal received by antenna#, (x_n, y_n) is the coordinate of the nth point radiation source, $F_\#$ is the normalized antenna pattern of antenna#, and the index part is the most critical wave path difference in synthetic aperture imaging. According to the geometric relationship diagram shown in Fig. 1, The exact expressions of the distances R_n^c and R_n^ι can be expressed as:

$$R_n^c = \sqrt{(x_n - X_C)^2 + (y_n - Y_c)^2 + R^2} \tag{2}$$

$$R_n^\iota = \sqrt{(x_n - X_\iota)^2 + (y_n - Y_\iota)^2 + R^2} \tag{3}$$

Normally, in order to separate the variables, it is necessary to perform Taylor expansion on the distances R_n^c and R_n^ι. Then ΔR in the exponential term can be expressed as:

$$\begin{aligned} \Delta R_{n,c,\iota} &= R_n^c - R_n^\iota \\ &\approx \left(R + \frac{(x_n - X_C)^2 + (y_n - Y_c)^2}{2R}\right) \\ &\quad - \left(R + \frac{(x_n - X_\iota)^2 + (y_n - Y_\iota)^2}{2R}\right) \\ &= \frac{x_n (X_\iota - X_C) + y_n (Y_\iota - Y_c)}{R} + \frac{(X_c^2 + Y_c^2) - (X_\iota^2 + Y_\iota^2)}{2R} \end{aligned} \tag{4}$$

In far-field imaging, the target is usually located in the far-field region, and the second term in the above formula can usually be approximated to zero. However, in near-field imaging, the imaging distance and the antenna aperture are relatively close in value. The influence of the second term on near-field imaging cannot be ignored. Bring Eq. (4) into Eq. (1) to get:

$$\begin{aligned} V_{C,l} &= \sum_{n=1}^{N} T(n) F_c F_\iota^* \\ &\quad e^{-jK\left[\frac{x_n(X_\iota - X_C) + y_n(Y_\iota - Y_c)}{R} + \frac{(X_c^2 + Y_c^2) - (X_\iota^2 + Y_\iota^2)}{2R}\right]} \end{aligned} \tag{5}$$

Then rewrite Eq. (5) into matrix form:

$$V_{M\times 1} = G_{M\times N} T_{N\times 1} \tag{6}$$

$$\begin{aligned} G(m,n) &= F_c(x_n, y_n) F_\iota^*(x_n, y_n) \\ &\quad e^{j\pi\left[2x_n(X_{mc} - X_{m\iota}) + 2y_n(Y_{mc} - Y_{m\iota}) + X_{m\iota}^2 + Y_{m\iota}^2 - X_{mc}^2 - Y_{m\iota}^2\right]/R\lambda} \end{aligned} \tag{7}$$

Where V is the measured visibility function, T is the brightness temperature data of the scene, G is the imaging matrix, (X_{mc}, Y_{mc}) and $(X_{m\iota}, Y_{m\iota})$ are the coordinates of antenna. The imaging method based on the G matrix is to perform image inversion by solving G. The more accurate the G matrix, the better the inversion effect. In the same way, we can also derive the MFFT imaging formula based on phase correction from Eq.(5).

$$V(\nu, h) = e^{-\varphi(\nu,h)} \iint T^0(x,y) e^{jk(\nu x + hy)} dxdy \tag{8}$$

$$T^0(x,y) = IFT_2[V(\nu,h) e^{\varphi(\nu,h)}] \tag{9}$$

Where $\nu = k(X_c - X_\iota)/R$, $h = k(Y_c - Y_\iota)/R$ is the spatial frequency domain variable. $\varphi(\nu,h) = k(X_C^2 + Y_C^2 - X_\iota^2 - Y_\iota^2)/2R$ is the phase correction term. $T^0(x,y)$ is the approximate brightness temperature. IFT_2 stands for two-dimensional inverse Fourier transform. The MFFT method is dedicated to solving the approximate brightness temperature distribution as an approximate solution of the brightness temperature distribution.

Both of these imaging methods are based on their own inversion model, using numerical inversion method to optimize the reconstruction of the target image. The reconstruction accuracy largely depends on the accuracy of their inversion model. However, due to some simplified approximations in model construction, the actual SAIR inversion model often has a certain description error. In addition, due to specific environmental constraints in actual imaging applications. There are often situations where it is difficult to accurately obtain some imaging parameters. Thus, the millimeter wave image reconstructed by the traditional imaging method usually has inevitable reconstruction errors.

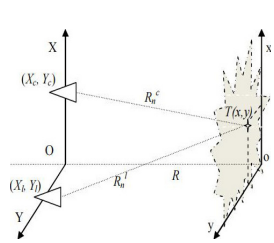

Fig. 1 Interference measurement schematic.

2.2 Description of the FCIN for Near-Field

In view of the particularity of near-field SAIR and the object full connectivity between visibility function and brightness temperature image. FCIN method is proposed to realize higher-precision SAIR imaging inversion from the sparse

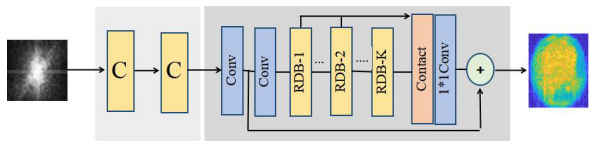

Fig. 2 Network structure of FCIN.

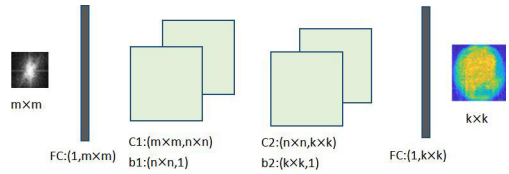

Fig. 3 Feedforward imaging network.

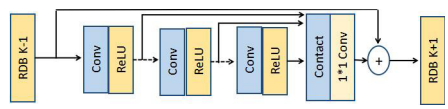

Fig. 4 Residual dense denoising network.

visibility function. The network structure of FCIN is shown in Fig. 2.

Our near-field millimeter wave imaging network is mainly composed of two parts, the feedforward imaging network and the residual dense denoising network. The extended dimension network is designed to reconstruct millimeter wave images from sparse visibility functions in feedforward imaging network. Then a denoising network based on the residual dense network is used to denoise and enhance the preliminary imaging results for improving the reconstruction accuracy further.

In feedforward imaging network, the full-connected method is used to perform dimensional convolution and feature extraction on the visibility function. The two-stage expansion convolution is used as a hidden layer to extract the mapping relationship between the spectrum domain of visibility function and image domain of millimeter wave image result. The expanded dimensional convolution model of the first and second stage is:

$$\begin{aligned} T1_{m\times m} &= C1_{m^2,n^2} \bullet V_{n^2} + b1 \\ T2_{k\times k} &= C2_{k^2,m^2} \bullet T1_{m^2} + b2 \end{aligned} \tag{10}$$

Where C1 is the extended dimension convolution coefficient of the first layer and C2 is the extended dimension convolution coefficient of the second layer, and its initial value will be set according to the initial measurement data of the imaging system. Here, the value of m is set to 50 and the value of k is set to 100. These parameters can be set higher to obtain better imaging effect according to actual needs. In this paper, these three parameters are set by considering the learning time and algorithm performance according to the current hardware environment.

In the framework of deep learning, Convolutional neural network has fewer connections and parameters. Due to the sparse connection, the neurons in the convolution layer are only connected to some of their adjacent layers. This connection structure improves the stability and generalization ability of the network structure. However, it will lead to the loss of some valuable features information and ignore the correlation between the whole and part, which leads to its optimal accuracy lower than that of the feedforward neural network. Considering the limited visibility function of near-field SAIR, we choose feedforward neural network instead of convolutional neural network to complete the image reconstruction task. Feedforward imaging network structure as shown in Fig. 3.

Since the feedforward neural network with two-layer extended dimension network is difficult to describe the actual imaging process absolutely and accurately, there are some errors and interferences in the initial reconstructed image of feedback network. Therefore, we use the residual dense network to denoise and enhance the image further. The residual dense network can effectively reduce the computational complexity of the network, reduce a large number of network parameters and shorten the computing time. In the residual dense denoising network, the cascaded intensive residual network structure will be used to complete the local feature learning and noise removal of the image. The key residual intensive module residual dense block composition structure is shown in Fig. 4. Through each convolution, the dense connection between layers fully mines the local feature information of the image, and uses the residual learning method to learn and store the feature information extracted by all convolutional layers, which can improve the learning efficiency of the network while ensuring the image denoising performance.

We use numerical simulation to construct the SAIR imaging dataset (10,000 pairs of image-visibility functions). We selected 10,000 images from ImageNet and sent them to the SAIR simulator to generate the corresponding visibility functions.We randomly select 100 images and visibility functions as the test set and the remaining are used as the training set. During training, the visibility function is used as the input of the network, and the high-precision millimeter-wave images are expected as the output of the network. The loss function is the total of mean square error (MSE) and peak signal-to-noise ratio (PSNR) between the real scene and the reconstructed image. After about 10,000 pieces of training, the error between the actual value and the predicted value is reduced to a relatively small value. The RMS Prop algorithm was used to minimize the loss function with minibatches of size 100, learning rate 0.0001, momentum 0.0, and decay 0.9. All the networks were trained on the tensorflow framework of Python3.7 using GPU (RTX 2080Ti) on the workstation.

3. Simulation and Results

For further demonstrating the effectiveness of the FCIN method, two groups of two-dimensional imaging simulation experiments from test set are performed here. The main sim-

Table 1 Simulation parameters of SAIR.

Parameters	Values	Parameters	Values
Wavelength	3 mm	Antenna aperture	0.4 m
Array size	50 ∗ 50	Imaging distance	6 m
Antenna spacing	1 cm	Source spacing	7 mm

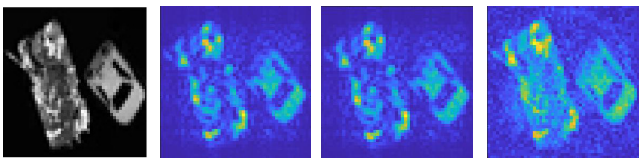

(a) tank&car (b) MFFT. (c) G-matrix (d) FCIN.

Fig. 5 The reconstructed images of tank&car scene.

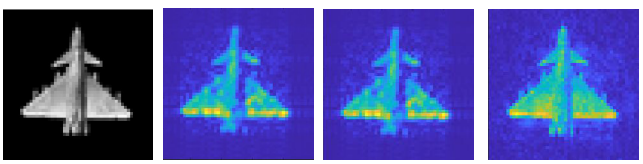

(a) airplane (b) MFFT. (c) G-matrix. (d) FCIN.

Fig. 6 The reconstructed images of airplane scene.

ulation parameters of SAIR simulator are listed in Table 1.

The tank&car and airplane are selected as simulated test images. The brightness temperature distribution of the target scene are shown in Fig. 5 (a) and Fig. 6 (a). In order to simulate the detection process of the actual SAIR, the gray value is used as the radiation intensity of the discrete radiation source. The signal received by the array antenna is obtained by integrating the generated millimeter wave radiation signal, then the visibility function is obtained through the complex correlation calculation between the antenna pairs. Then, the images are reconstructed by the imaging methods from the measured visibility function. The imaging results of the MFFT method, G-matrix method, and the proposed FCIN-SAIR method are shown in Fig. 5 and Fig. 6.

It can be found that because the MFFT method makes the visibility function and the brightness temperature image meet the approximate Fourier transform. The correction process is simple, but the accuracy is low and its reconstructed image has large noise pollution. Compared with the MFFT method, regularization method based on G-matrix uses the regularization method to optimize the numerical iteration, which has higher accuracy, can remove most of the noise and effectively restore the target information. However, the G-matrix model itself has some errors, so its reconstructed image exists the phenomenon of inconspicuous contours and blurred details, and the sharpness of the target is still poor. FCIN method directly establishes the mapping relationship between the visibility function to the millimeter wave, avoiding interference factors such as background noise, system parameters and imaging model errors caused by the establishment of inversion model. Moreover, the feedforward neural network is used to infinitely approximate the actual imaging process. This makes the contour and detail of the reconstructed image more clear and recognizable, the image noise is effectively filtered, and its imaging accuracy is obviously better than the MFFT method and the G-matrix method. In order to objectively evaluate the accuracy of the imaging results, PSNR and RMSE are calculated, and the results are shown in Table 2. The FCIN method has the smallest RMSE and the largest PSNR. The results show that the imaging results of the proposed FCIN method are significantly better than the MFFT method and the G-matrix method.

Table 2 Comparison of reconstruction quality between the images.

Scene	Evaluation criterion	MFFT	G-matrix	FCIN
tank&car	RMSE	44.7982	38.5052	28.7010
	PSNR	15.7236	16.1488	20.2075
airplane	RMSE	44.2723	40.0915	24.6158
	PSNR	16.2768	18.2133	20.3065

Table 3 Reconstruction time comparison.

Scene	MFFT	G-matrix	FCIN
tank&car	36 s	108 s	4 s
airplane	36 s	103 s	4 s

In addition, inversion time is an important consideration. Although we use a lot of data for training, it takes a lot of time. The inversion process only need to call the network model and use, the imaging inversion of FCIN is very fast. The MFFT method and the G-matrix method require a large amount of data calculation in the inversion process, which is very time-consuming. Table 3 shows the time required for the imaging inversion of the three methods. It can be found that the MFFT method and the G-matrix method consume a long time and cannot realize real-time imaging, while FCIN method adopts a shorter time and can realize real-time imaging.

4. Conclusion

In order to reconstruct high-precision millimeter wave image, this paper proposes a new FCIN imaging method. According to the particularity of near-field SAIR, feedforward fully connected neural network is used to reconstruct high-dimensional millimeter wave image from sparse sampled visibility function. Then the dense residual denoising network is used for further improve image quality, and finally achieve higher precision near-field SAIR sparse reconstruction. Experimental results show that FCIN method has great advantages in imaging accuracy and reconstruction time.

References

[1] R. Appleby and R.N. Anderton, "Millimeter-wave and submillimeter-wave imaging for security and surveillance," Proc. IEEE, vol.95, no.8, pp.1683–1690, Aug. 2007.

[2] M. Martin-Neira, D.M. LeVine, Y. Kerr, N. Skou, M. Peichl, A. Camps, I. Corbella, M. Hallikainen, J. Font, J. Wu, S. Mecklenburg, and M. Drusch, "Microwave interferometric radiometry in remote

sensing: An invited historical review," Radio Science, vol.49, no.6, pp.415–449, June 2014.

[3] C.S. Ruf, C.T. Swift, A.B. Tanner, and D.M. Le Vine, "Interferometric synthetic aperture microwave radiometry for the remote sensing of the earth," IEEE Trans. Geosci. Rem. Sens., vol.26, no.5, pp.597–611, Sept. 1988.

[4] A. Camps, J. Bara, I.C. Sanahuja, and F. Torres, "The processing of hexagonally sampled signals with standard rectangular techniques: Application to 2-D large aperture synthesis interferometric radiometers," IEEE Trans. Geosci. Remote. Sens., vol.35, no.1, pp.183–190, Jan. 1997.

[5] N. Duffo, I. Corbella, F. Torres, A. Camps, and M. Vall-llossera, "Advantages and drawbacks of near field characterization of large aperture synthesis radiometers," Proc. 8th Specialist Meeting on Microwave Radiometry and Remote Sensing Applications, University La Sapienza, Rome, pp.24–27, 2004.

[6] J. Chen, Y. Li, J. Wang, Y. Li, and Y. Zhang, "An accurate imaging algorithm for millimeter wave synthetic aperture imaging radiometer in near-field," Prog. Electromagn. Res., vol.141, pp.517–535, 2013.

[7] Y. Zhang, Y. Ren, W. Miao, Z. Lin, H. Gao, and S. Shi, "Microwave SAIR imaging approach based on deep convolutional neural network," IEEE Trans. Geosci. Rem. Sens., vol.57, no.12, pp.10376–10389. Aug. 2019.

[8] A. Tanner, B. Lambrigsten, T. Gaier, and F. Torres, "Near field characterization of the GeoSTAR demonstrator," 2006 IEEE International Symposium on Geoscience and Remote Sensing, pp.2529–2532, 2006.